UCRL-ID-122899

Effect of Radiation on the Mechanical Properties of Topopah Spring Tuff

RECEIVED
AUG 16 1996
OSTI

S. C. Blair
J. M. Kelly
O. Pine
R. Pletcher
P. A. Berge

June 1996

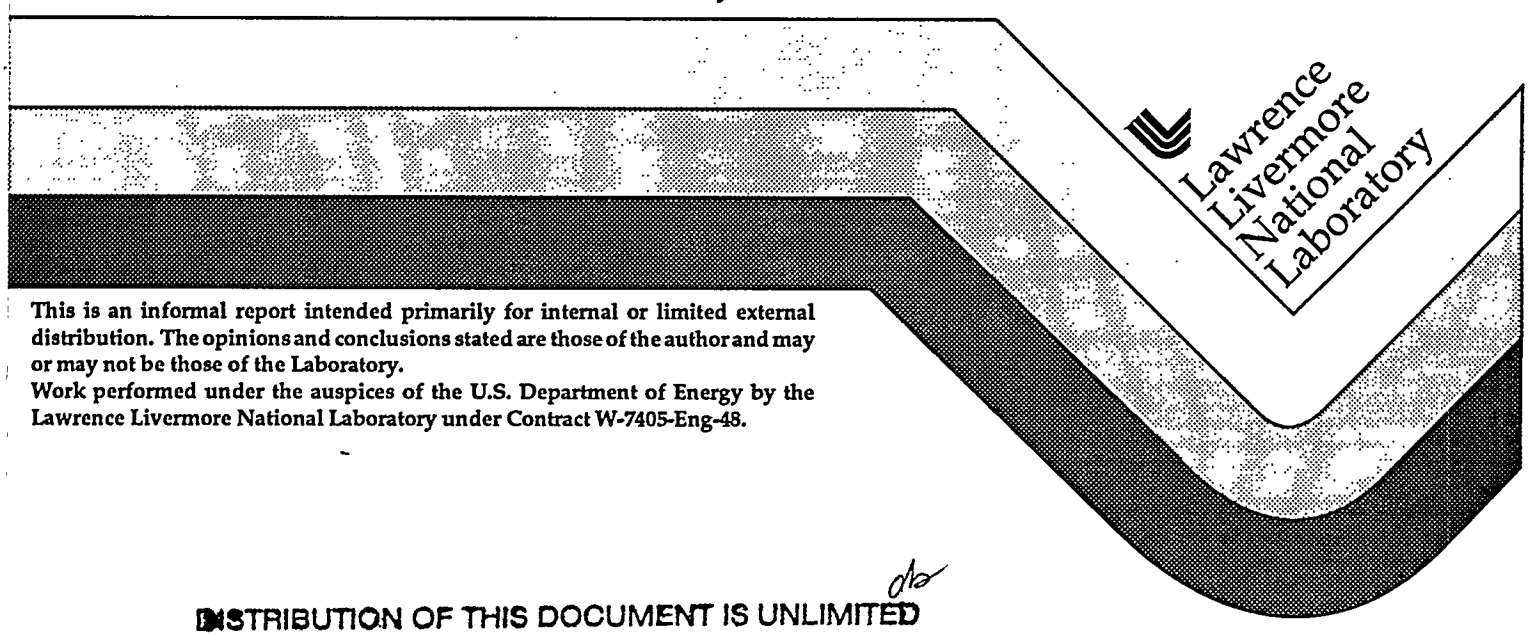

This is an informal report intended primarily for internal or limited external distribution. The opinions and conclusions stated are those of the author and may or may not be those of the Laboratory.
Work performed under the auspices of the U.S. Department of Energy by the Lawrence Livermore National Laboratory under Contract W-7405-Eng-48.

DISTRIBUTION OF THIS DOCUMENT IS UNLIMITED

MASTER

DISCLAIMER

This document was prepared as an account of work sponsored by an agency of the United States Government. Neither the United States Government nor the University of California nor any of their employees, makes any warranty, express or implied, or assumes any legal liability or responsibility for the accuracy, completeness, or usefulness of any information, apparatus, product, or process disclosed, or represents that its use would not infringe privately owned rights. Reference herein to any specific commercial product, process, or service by trade name, trademark, manufacturer, or otherwise, does not necessarily constitute or imply its endorsement, recommendation, or favoring by the United States Government or the University of California. The views and opinions of authors expressed herein do not necessarily state or reflect those of the United States Government or the University of California, and shall not be used for advertising or product endorsement purposes.

This report has been reproduced
directly from the best available copy.

Available to DOE and DOE contractors from the
Office of Scientific and Technical Information
P.O. Box 62, Oak Ridge, TN 37831
Prices available from (615) 576-8401, FTS 626-8401

Available to the public from the
National Technical Information Service
U.S. Department of Commerce
5285 Port Royal Rd.,
Springfield, VA 22161

DISCLAIMER

Portions of this document may be illegible in electronic image products. Images are produced from the best available original document.

Effect of Radiation on the Mechanical Properties of Topopah Spring Tuff

S. C. Blair, J. M. Kelly, O. Pine,
R. Pletcher, and P. A. Berge

June 4, 1996

Contents

Effect of Radiation on the Mechanical Properties of Topopah Spring Tuff

Introduction and Background

This report presents results of a suite of uniaxial compressive tests conducted to provide laboratory data to determine how radiation affects the compressive strength of Topopah Spring Tuff, which is the rock type for the proposed geologic repository at Yucca Mountain, in Nevada. The repository would be designed for storing spent fuel and other high-level radioactive wastes. We need to better understand what effect radiation has on the compressive strength of this type of rock because emplacement of radioactive waste may impose a radiation field on the rock that is exposed in the emplacement drifts and other excavations associated with the proposed repository. Thus, we must determine whether exposure to radiation will alter the mechanical strength or other geomechanical properties of the rock in the very near-field region of the repository. Until now, data describing the effect of radiation on tuff from the potential repository horizon have not been available.

The approach taken was to precisely measure rock behavior in uniaxial compression on irradiated and non-irradiated samples of Topopah Spring Tuff. Identical procedures were used for preparing and testing the samples tested for radiation effects and those that were not irradiated, except for the exposure to gamma radiation. Results for the irradiated and non-irradiated samples were then compared.

In this report, we describe the sample preparation and testing methodology, and provide preliminary results in the form of stress-strain curves and tabulated strength and modulus values. Preliminary conclusions are also presented.

Samples of Topopah Spring Tuff were obtained from a boulder excavated from Fran Ridge, near Yucca Mountain at the Nevada Test Site. Samples for the experiments were prepared as right circular cylinders according to the specifications recommended by the American Society of Testing and Materials (ASTM). The samples have a length-to-diameter ratio of 3:1, with a 7.62-cm (3-in.) length and 2.54-cm (1-in.) diameter. The density of the samples is approximately 2.3 g/cm^3.

One statistical method that has been evaluated for analyzing the effect of radiation is known as blocking. A block is a unit of sample material within which the variation of some attribute is less than its variation between blocks.

Treatment comparisons are then made within blocks rather than across blocks. The different blocks can be viewed as independent replications of the comparison. The block size in our experiments is two, so the method is also known as the method of matched pairs. For each pair, one sample is exposed to a massive dose of gamma radiation, while the second sample acts as a control. For validity, the two samples must be treated identically in all other respects. Any radiation effect is detected by comparing the measured parameter between the members of a pair.

Samples were irradiated with gamma radiation at the ^{60}Co irradiation pool at Lawrence Livermore National Laboratory (LLNL). To evaluate the effect of radiation, we used a gamma-irradiation method similar to that used by Durham et al. (1986). Control samples were handled in the same manner as the irradiated samples except for the irradiation process. The total dose of gamma radiation was monitored by time/dose.

The irradiated samples received the dose at a higher rate than is expected in a repository. However, the dose-rate dependence of the damage is expected because two individual gamma-ray interactions in the same incremental volume of material are improbable within a period equal to the relaxation time of the electrons at the dose rate used. If a time-dependent recovery of damage should occur, however, laboratory scaling to shorter times would tend to increase damage in the laboratory samples for a given absorbed dose. The approximate time between irradiation and mechanical testing was 36 days. The uniaxial experiments were performed at the LLNL rock mechanics laboratory.

Methods and Procedures

In this report, we describe our study to determine what effects gamma radiation has on the geomechanical properties of rock samples from the proposed repository horizon at Yucca Mountain. This report is based on procedures presented by Durham et al. (1986), who did a study on the mechanical effects radiation has on the mechanical properties of granite, as well as on ASTM procedures D-2664-86, D-2938-86, D3148-86, and D4543-85 (when applicable). A rock sample adequate for preparing 40 to 50 1- × 3-in. cores was obtained from a boulder from Fran Ridge at the Nevada Test Site. Unconfined compression tests were performed on 39 1- × 3-in. cylindrical core samples. Fifteen samples were subjected to a 9.5-MGy (0.9-Grad) dose of gamma irradiation from a ^{60}Co source over a 47-day period. The remaining samples were held as control samples. Each sample was then loaded in uniaxial compression until it failed.

Preparation of Cores

A piece of outcrop material that was cut from a boulder quarried from Fran Ridge was used as a source for core samples. This piece of tuff, which measured 12 in. × 12 in. × 4 in., was chosen for its homogeneity and its thickness (4 in.), because it was flat and true on top and bottom, and because it was big enough to provide 40 to 50 cores. This piece of outcrop material was too large to fit on the available coring machine, so it was cut into three 4-in. × 4-in. × 12-in. slabs that fit on the coring table.

Coring. As many cores as possible were taken from each 4-in. × 4-in. × 12-in. slab. The coring equipment consisted of:

- A large drill press.
- A water swivel.
- A 1-in., diamond-impregnated core drill.
- A vise.
- Filtered, deionized water (DI H_2O) used as a coolant and to remove cuttings from coring.

As each core was taken, it was given a number starting at 1 and ending at 44. The number was also written on the slab for future reference. After coring, each core sample was inspected for flaws, such as large vugs and open fractures. Five samples were unsuitable for compressive strength testing because we found large cracks, vugs, or other irregularities. These were samples #18, #24, #27, #36, and #38. All of the remaining cores were rinsed with DI H_2O to remove fine dust.

To obtain the precise length of the cores in an efficient way, we cut them in two stages. First, an Isomet precision saw with a 4.5-in. diamond-impregnated blade was used to cut the cores to a length of about 3.1 in., and DI H_2O was used as a coolant. After one end of the core was cut, the length was measured with digital calipers that read accurately to 0.001 in. When the ends were sawed off, the length of the cores was 3.100 in. The final length was obtained by grinding core ends flat and parallel, using a precision grinder. The cores were again rinsed with DI H_2O.

Prior to grinding, each core was measured with digital calipers reading to 0.001 in. Lines were drawn with an indelible marking pen on the ends of the core sample to assure that the entire surface was ground. Once one end of the core was ground, it was rinsed with DI H_2O and measured again to determine the amount of material to be ground to obtain a finished length of 3.000 in. After grinding, each core was rinsed again with DI H_2O. The cores were air dried for

1 hour, and the ends were measured to make sure that they were parallel within 0.001 in. (25 μm).

Drying of cores. All core samples were placed in a vacuum oven set at a temperature of 35°C and a vacuum of –10 in. of Hg. A tray of desiccant was placed in the oven to absorb any condensation or moisture. Cores were weighed every 24 hours to the nearest 0.001 g until the weight loss was less than 0.1 g for at least 3 consecutive days. Table 1 lists the dimensions, weight, and dry bulk density of the core specimens used in this study, which shows that the samples were quite uniform in both size and density.

Pairing of cores. The next step was to pair the cores that had similar appearance and that had similar cracks and vugs. We formed 19 pairs (Table 2), and because we had an odd number of usable samples, sample #21 could not paired. This sample was used to test the apparatus. Fifteen pairs were chosen for the radiation study; in Table 2, these are pairs a through o. This study was limited to 15 pairs because the canister used to irradiate the samples would hold only 15 cores. The remaining 4 pairs (pairs p through s) were used with sample #21 as a control group.

For the 15 pairs used in the irradiation study, a coin was tossed to determine which sample in each of these pairs would be irradiated. In Appendix A, we describe the samples in each pair tested in the radiation study.

Irradiation of cores. The samples were irradiated with gamma radiation at the ^{60}Co irradiation pool at the LLNL Standards and Calibrations Laboratory. The samples were irradiated dry in a waterproof chamber (gamma cell). The size of the sample chamber allowed us to irradiate 15 samples at a time. The samples were arranged in 3 layers with 5 samples per layer. The chamber was lowered into the source, which lies at the bottom of a 6-m-deep pool of deionized water. The source is made up of 72 ^{60}Co rods that are 190 mm long and 110 mm in diameter, and are arranged in a circle. A gamma-ray dose of 9 ± 1 MGy (0.9 Grad) was used to irradiate samples. The control samples were placed in a similar container and set next to the irradiation pool.

Because of other experiments and calibrations, we had to remove the samples from the radiation field for short periods of time. The cores were irradiated according to the schedule given in Table 3.

When the radiation exposure was completed, we found that the 15 irradiated cores had developed a distinctive gray color. This finding was not surprising because rock with high quartz content develops color centers because displaced electrons and holes are trapped by impurities and crystal defects. In most cases, the color change can be reversed by putting the sample under an ultraviolet (UV) light source.

Table 1. Sample descriptions.

Sample	Length (in.)	Diameter (in.)	Dry weight (g)	Dry density[a] (g/cm^3)
1	3.000	1.000	89.830	2.33
2	3.003	1.000	88.167	2.28
3	2.998	1.000	89.131	2.31
4	2.999	1.000	90.117	2.33
6	3.000	1.000	89.973	2.33
7	2.997	1.000	90.202	2.34
8	2.998	1.000	90.813	2.35
9	3.000	1.000	90.556	2.35
10	2.998	1.000	90.316	2.34
11	3.000	1.000	90.246	2.34
12	3.000	1.000	89.993	2.33
14	3.000	1.000	90.298	2.34
15	3.000	1.000	90.213	2.34
16	2.999	1.000	90.107	2.33
20	3.000	1.000	90.196	2.34
22	3.000	1.000	91.215	2.36
25	3.000	1.000	90.207	2.34
26	3.000	1.000	89.489	2.32
28	3.000	1.000	90.302	2.34
30	3.000	1.000	89.078	2.31
31	3.000	1.000	90.144	2.33
32	2.999	1.000	89.908	2.33
33	3.000	1.000	90.259	2.34
35	3.000	1.000	89.463	2.32
37	2.995	1.000	88.608	2.30
39	3.000	1.000	90.160	2.34
40	2.999	1.000	90.268	2.34
41	2.999	1.000	89.764	2.33
43	2.995	1.000	89.217	2.31
44	3.002	1.000	90.239	2.34

[a]Average density = 2.33 g/cm^3.

Table 2. Sample Pairs

Pair	Control	Irradiated
a	1	43
b	4	8
c	7	28
d	9	10
e	11	16
f	12	37
g	14	22
h	20	6
i	25	2
j	26	40
k	30	3
l	31	39
m	33	32
n	41	35
o	44	15
p	5	29[a]
q	13	42[a]
r	17	34[a]
s	19	23[a]

[a]Not irradiated.

Table 3. Schedule of irradiation

	Date	Time of day	Total time (days)
In	17 Mar 1995	3:15 p. m.	
Out	28 Mar 1995	9:40 a. m.	10.8
In	29 Mar 1995	8:10 a. m.	
Out	7 Apr 1995	4:20 p. m.	9.3
In	10 Apr 1995	8:40 a. m.	
Out	27 Apr 1995	2:00 p. m.	17.2
In	12 May 1995	4:20 p. m.	
Out	22 May 1995	8:30 a. m.	9.7
Total exposure:	47.0 days in pool		
	9.5 MGy maximum		

Uniaxial Test Apparatus

The test apparatus used for this experiment consisted of the following components:

- 100-ton-capacity reaction frame with a 50-ton hydraulic ram.
- Strain gauged "dog bone" load cells (85,000 lb), for axial displacement.
- Direct current displacement transducers (DCDT).
- Alignment fixtures.
- Standard single upper platen.
- Swivel lower platen.
- Three-mil foil shims.

The test assembly from bottom to top consisted of a precision swivel platen, a core specimen, a top platen, and a load cell. This test assembly was mounted inside a 100-ton reaction frame that was equipped with a 50-ton hydraulic loading ram, which was used to apply the uniaxial compression. The ram is mounted in the bottom of the opening in the reaction frame and moves upward. Two displacement transducers were mounted to the reaction frame, with the sensor rods resting on the cap of the hydraulic ram to monitor its movement. The apparatus is a slight modification of the apparatus used by Durham et al. (1986) to test for the effect of radiation on Climax granite.

Procedure

The test cores were aligned and fixed in place using two removable fixtures. With the alignment fixtures still in place, the operator raised the ram to near closure of the column, then checked for and corrected any misalignment. With the column satisfactorily aligned, the operator loaded the sample to 2 ± 0.5 MPa. At that point, the operator removed the two alignment fixtures. Loading of the test core was controlled automatically at a constant strain rate of 10^{-5} s^{-1}. The sample was loaded to failure.

Data-Acquisition System

An automatic data-acquisition system was used for recording data in the uniaxial compressive tests. The system read the load cell input and output voltages, and the output voltages from two displacement transducers. The data were recorded on an Apple Macintosh IIcx computer using National Instruments' software LabView version 3.1 and a LabView virtual instrument (vi) program written for this purpose. This vi converted the load cell output

voltages into force in pounds and displayed both the load and displacement on the Macintosh monitor. The data were also stored, with the date and time, on disk in an ASCII file.

Data Reduction and Analysis

Axial load recorded in pounds was converted to axial stress by incorporating the cross-sectional area of the sample. (We did not correct the cross-sectional area as the specimen deformed.) The outputs from the displacement transducers were converted into inches of displacement. The strain was computed from the displacements and the length of the samples. Two displacement measurements were made for each test, and displacements and strains were computed using the average of the two measurements. Once the data were reduced, stress/strain plots were made. Then values for the peak strength and Young's modulus were determined and tabulated, and the averages computed.

Results

Table 4 lists results from the uniaxial tests on each samples in pairs a through o, including peak strength, Young's modulus, irradiation status, and general comments on the behavior of the sample during testing. In Table 4, paired samples are grouped between rules. Appendix B shows stress-strain curves plotted for each of the pairs tested. In these figures, the solid line represents the control sample, and the heavy dashed line represents the irradiated sample. These figures show that most of the samples behaved in a linear elastic manner up to the point of brittle fracture, and that the Young's modulus for matched cores was similar. Stress-strain curves for some samples do show nonlinear behavior at stress levels below the peak stress (these include pair b #4, and pair h #20 as well as others). Moreover, for many of the pairs, the behavior for each of the samples is quite similar, but for some of the pairs, dissimilar behavior is observed for the two samples (see pairs i and j). This finding is discussed later in the report.

Table 5 lists mean values of peak strength and Young's modulus for the cores in the 15 matched pairs (pairs a–o) used in the radiation study. These values indicate that the irradiated samples had a mean strength of 139 MPa ± 73.4 MPa, whereas the control samples in these pairs had a mean peak strength of approximately 154 MPa ± 36.1 MPa. These values for peak strength are consistent with those reported elsewhere for welded tuff (Price et al., 1982). The large amount of scatter in the values is also expected and is generally attributed to the heterogeneity in the form of cracks and vugs present in the rock.

Table 4. Results from the uniaxial tests on each sample in pairs a–o.

Pair	Sample ID No.	Peak strength (MPa)	Young's modulus (GPa)	Rad. (Y/N)	Comments[a]
a	1	170.5	25.4	N	Chipping at 122, 158, and 166 MPa.
	43	123.0	23.3	Y	Vertical crack formed through a preexisting vug near 100 MPa.
b	4	135.6	24.6	N	A sliver cracked off at about 87 MPa.
	8	221.2	27.1	Y	No chipping or cracking before failure.
c	7	191.1	27.8	N	No cracking or chipping before failure.
	28	213.4	25.9	Y	No cracking or chipping before failure.
d	9	58.9	17.9	N	Failure along preexisting fracture.
	10	150.5	21.2	Y	Preexisting crack opened at about 122 MPa.
e	11	192.6	27.5	N	Ram pressure increased somewhat slower than in other tests.
	16	151.9	26.1	Y	No cracking or chipping before failure.
f	12	164.5	25.0	N	No cracking or chipping before failure.
	37	63.0	23.9	Y	See comments in Appendix A.
g	14	201.6	26.7	N	Chipping at about 193 MPa.
	22	236.0	26.4	Y	No cracking or chipping before failure.
h	20	158.3	27.1	N	Cracking and chipping around 148 MPa.
	6	204.0	26.8	Y	A chip fell off at 160 MPa.
i	25	149.0	25.4	N	Chipping at about 131 MPa.
	2	47.9	6.8	Y	Failure along preexisting fracture.
j	26	128.4	24.2	N	Chipping at about 122 MPa.
	40	76.3	19.0	Y	Chipping along a preexisting crack.
k	30	132.4	23.1	N	Large chips fell off; the test was paused and restarted.
	3	96.0	23.3	Y	Chipping at about 87 MPa.
l	31	116.8	22.7	N	Some cracking.
	39	31.9	21.0	Y	Failure along a large preexisting fracture.
m	33	168.3	23.2	N	No chipping or cracking before failure.
	32	213.0	26.6	Y	Cracking and chipping at about 193 MPa.
n	41	166.6	25.2	N	Chipping at about 140 MPa.
	35	51.3	22.5	Y	Failure due to preexisting crack.
o	44	174.1	27.7	N	No cracking or chipping before failure.
	15	205.8	27.3	Y	Chipping at about 193 MPa.

[a]See Appendix A for comments on each sample's initial condition.

Table 5. Average values for peak strength and Young's modulus for various groups of samples.

Samples	Rad. (Y/N)	Average peak strength (MPa)	Standard deviation	Average Young's modulus (GPa)	Standard deviation
Pairs a–o	Y	139.0	73.4	23.1	5.2
(15 pairs)	N	153.9	36.1	24.9	2.6
Homogeneous samples	Y	184.9	48.9	25.9	1.5
(9 pairs)	N	169.4	24.3	25.9	1.9
Heterogeneous samples	Y	70.2	38.4	19.1	5.7
(6 pairs)	N	130.7	36.8	23.4	2.6
Pairs p–s[a]	H	152.5	42.1	26.2	6.2
(4 pairs)	L	138.9	40.3	22.3	2.9

[a]For pairs p–s, H = high sample ID numbers, and L = low sample ID numbers. All H cores were treated as if they were irradiated, although they were not.

These values (shown graphically in Figure 1) indicate that radiation has no significant effect on the mean strength of the rock. However, the irradiated samples do show a wider variability in mean strength than that observed for the non-irradiated samples (see Table 5).

The Young's modulus values for pairs a–o also show no significant dependence on exposure to radiation (see Figure 2). However, again, the irradiated samples do show a slightly lower mean value and a larger standard deviation than the non-irradiated samples (Table 5).

As mentioned, for some of the pairs, the individual samples showed widely differing results. To further evaluate this behavior, we divided pairs a through o into two groups, termed the homogeneous and heterogeneous groups, based on stress-strain behavior for the pair. The homogeneous group contained pairs a, b, c, d, g, h, k, m, and o. The mean values for peak strength and Young's modulus for irradiated and non-irradiated samples in this group are listed in Table 5 and plotted in Figures 1 and 2. Nearly all of these samples failed by explosive brittle fracture. The values in Table 5 show that the mean peak strength for the irradiated samples in this group was slightly higher than that for the non-irradiated samples (Figure 1). Also, both irradiated and non-irradiated samples in this group had a higher mean peak strength than that determined for the total dataset. Again, the irradiated samples had a higher standard deviation (more scatter) in the mean peak strength than the non-irradiated samples. Values for

Young's modulus for the irradiated and non-irradiated samples in the homogeneous group were identical (Figure 2), with similar standard deviations. This result indicates that, for the homogeneous samples of welded tuff, radiation has little effect on the mechanical behavior in compression.

Values of mean peak strength and Young's modulus for irradiated and non-irradiated samples in heterogeneous pairs are also shown in Table 5 and in Figures 1 and 2. These results differ from those for the homogeneous group in that they indicate a significant difference between the mean peak strength observed for the irradiated and non-irradiated samples (Figure 1). The irradiated samples have a mean strength of approximately 70 MPa, and the non-irradiated have a mean strength of approximately 130 MPa. The values of Young's modulus (Figure 2) for the irradiated samples are also significantly lower than those for the non-irradiated samples in this group of pairs. Preliminary examination of the core descriptions and comments on testing for these samples indicates that, for many of the pairs, both samples in the pairs contained preexisting vertical or subvertical cracks. Also, for the irradiated samples, the failure occurred along

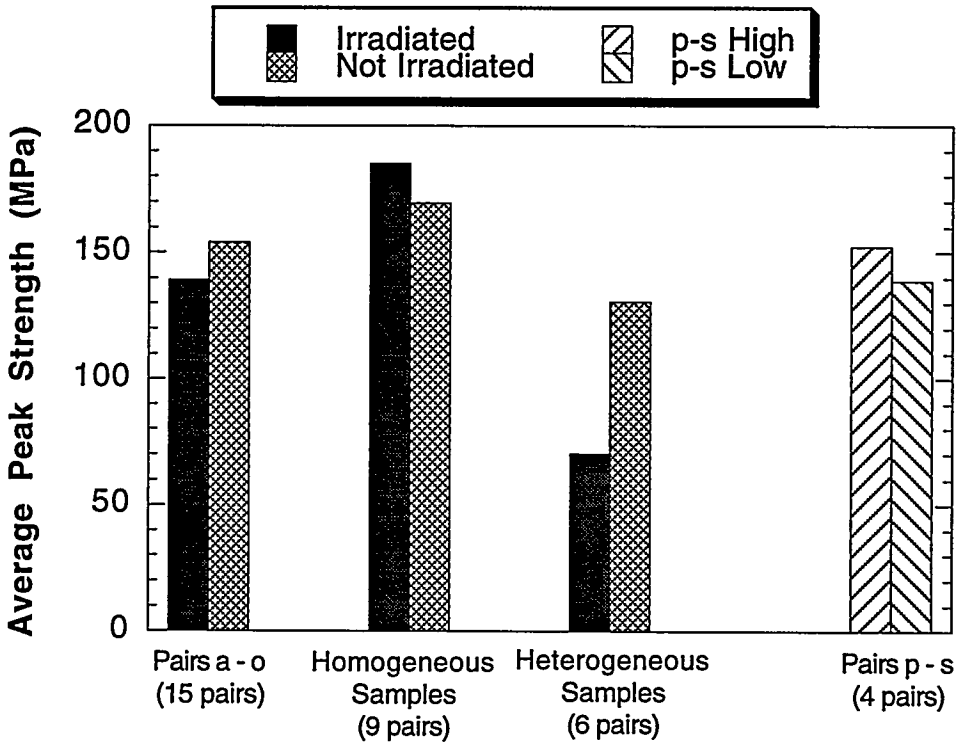

Figure 1. Histogram of peak strength for different groups of samples.

one of these preexisting cracks. For the non-irradiated samples in this group, failure occurred more frequently by catastrophic or explosive fracture.

Finally, Table 5 and Figures 1 and 2 also show values for the 4 pairs of cores that were held out of the radiation study (pairs p–s). For each of these pairs, the sample with the lowest number was analyzed as though it had been irradiated, even though it had not. Values of mean peak strength and Young's modulus for these pairs closely match the values tabulated for pairs a through o in the radiation study and thus further support the conclusion that radiation has no effect on the mechanical strength of the intact, uncracked welded tuff.

Discussion and Conclusions

Results reported in this preliminary report indicate that for homogeneous, uncracked samples of Topopah Spring Tuff from unit Tsw2 and quarried from

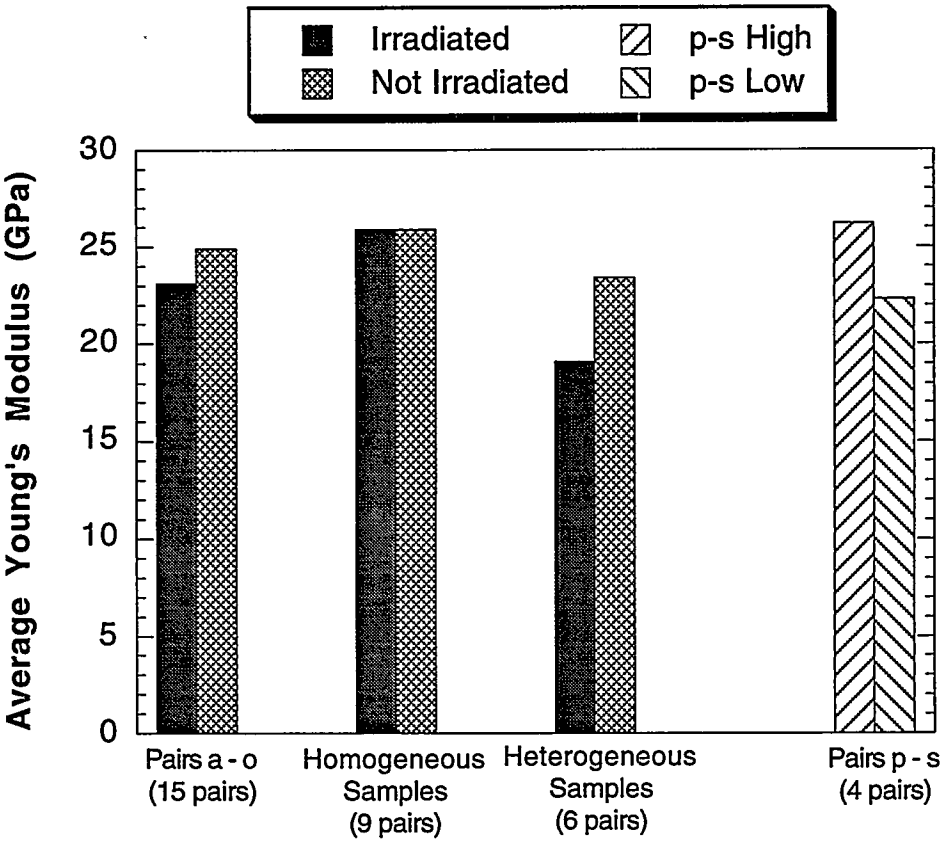

Figure 2. Histogram of Young's modulus values for different groups of samples

Fran Ridge, exposure to gamma radiation had no discernible effect on the unconfined compressive (peak) strength or the Young's modulus. However, results for samples that contained partially healed, preexisting vertical or subvertical cracks (the heterogeneous group) indicate that radiation may cause significant degradation of the strength and Young's modulus.

A possible explanation of the observed behavior for the heterogeneous pairs is that exposure to radiation weakened the cementing material in the cracks and fractures that were present in these samples, leading to the lower values of peak strength and Young's modulus. The cementing material is thought to be largely composed of carbonates. Several possible mechanisms can be postulated that could weaken the cementing material when it is exposed to radiation. We discuss two of the representative mechanisms.

One possible mechanism that could weaken a carbonate cementing material in a high radiation field is degradation of the carbonate by nitric acid formed by irradiation of moist air. The irradiated samples were enclosed in a sealed, stainless-steel vessel. When this vessel was lowered into the radiation pool, it contained air at atmospheric pressure and humidity along with the samples. The exposure of humid air to the radiation field would have caused some nitric acid to form (R. Van Konynenburg, personal communication, July 1995), and this acid could have attacked and weakened the carbonate cementing materials. This hypothesis could be evaluated by performing another similar set of experiments, but instead, flooding the irradiation vessel with an inert gas, such as argon, before exposing the samples to the radiation field.

A second mechanism is alteration of some of the hydrated minerals in the cementing material through radiolysis of the waters of crystallization (F. M. Doyle, personal communication, July 1995). The alteration would weaken the cementing material and thus degrade the compressive strength.

The results presented here are preliminary, and additional studies are warranted to evaluate whether radiation does weaken cementing materials in welded tuff. However, if this is a real phenomenon, it has significant implications for the behavior of rock in the near-field region of the proposed nuclear waste repository. The radiation field would be expected to affect only rock exposed on the surface of excavated drifts and to penetrate only a few centimeters into the rock. However, the rock in this region would also experience the highest temperatures and stresses in a repository as well as high humidity. Weakening of fracture-filling materials may cause unanticipated spalling, which may change the amount and nature of rock fragments that would come in contact with the waste containers. In addition, changes in fracture properties, such as fracture shear strength, compressibility, and permeability could also occur. Changes in

these properties would affect the thermomechanical and thermohydrological behavior of the rock in the very near-field region. In particular, changes in the shear strength of cementing material in fractures would enhance stress gradients that would occur within the rock mass and may affect rock mass behavior in unanticipated ways, including movement of rock blocks along fractures.

References

Durham, W. B., et al. (1986), *Nuclear and Chemical Waste Management*, 6, pp. 159–168.

Price, R. H., K. G. Nimick, and J. A. Zirzow (1982), *Uniaxial and Triaxial Compression Test Series on Topopah Spring Tuff*, Sandia National Laboratory, Albuquerque, NM, SAND82-1723.

Appendix A:
Description of Paired Core Samples

Pair	Core No.	Description
a	1	There is a major subhorizontal vug 2.9 to 3.2 cm from the top of the core with 1.0-mm aperture and some white mineral filling. There is a brown vug at the top of the core with white mineral filling.
	43	There is a subhorizontal vug 4.6 to 4.8 cm from the top of the core filled with light-pink altered material. The void has a 1-mm aperture. There are minor subhorizontal vugs with pink filling and micropores near the top of the core.
b	4	The core has a pink vug about 3 to 4 cm from the top and slight mottling of light brown and pink in the top 2 cm of the core. There are no large brown vugs, cracks, or voids.
	8	There is a minor dark-brown vug at the top of the core and a few minor subhorizontal brown vugs at the bottom of the core. There is no mottling, and there are no voids.
c	7	There is a large dark-brown vug 3.8 to 4.5 cm below the top of the core, and the vug is rimmed with a light-pink altered zone. There are several small (about 0.5-cm) subhorizontal brown vugs throughout the core. There are no significant voids and no significant mottling.
	28	There is a large dark-brown vug 3.0 to 4.2 cm below the top of the core. This vug is streaked with pink altered zones. There are several small (0.5-cm) brown vugs and minor mottled regions in the core. Some minor vugs contain small pores, but there are no significant cracks.
d	9	There is a partly open subvertical hairline to 0.5-mm crack through the entire core. A brown vug at the top of the core is surrounded by pink and dark-brown altered zones. There are minor subhorizontal pink and brown inclusions 1.0 to 1.3 cm from the top of the core, 2.0 to 2.5 cm from the top of the core, and 6.0 to 6.5 cm from the top of the core.
	10	There is a healed hairline vertical crack through the entire core. There are small dark-brown vugs 2.2 to 2.9 cm from the top of the core and 6.4 to 7.1 cm from the top of the core. There is a subhorizontal light-brown vug 5.2 to 5.5 cm from the top of the core.

Pair	Core No.	Description
e	11	There is a large dark-brown vug with a pink altered rim, 1.8 to 2.7 cm below the top of the core. There is another large dark-brown vug 3.9 to 4.5 cm below the top of the core with a pink altered zone surrounding the brown vug. There is a large dark-brown vug 0.4 to 1.2 cm below the top of the core. There is no mottling, and there are no significant cracks or large voids in the core.
	16	There is a small brown vug 0.6 to 1.1 cm below the top of the core. There is slight mottling near the top of the core. There is a very large dark-brown vug 5.7 to 6.9 cm below the top of the core, with a pink altered zone around most of the brown vug. There are no significant cracks or large voids in the core.
f	12	Core has an open horizontal vug about 3.5 to 4.0 cm from the top with an aperture of about 1 to 2 mm. There is a dark-brown inclusion about 1.4 to 2.2 cm from the top. There is a large pink inclusion with a hairline horizontal crack about 4.5 cm below the top.
	37	Core has subhorizontal void about 2 to 3 cm from the top. The aperture is 1 to 2 mm with some pink and white mineral filling. Another horizontal vug is 0.3 cm from the top of the core with an aperture of 1 mm. The core has a large gray and orange vug 1.4 to 2.8 cm from the top. This vug has horizontal cracks having hairline to 0.5-mm apertures. The top of the core is mottled pink and light grayish-brown.
g	14	There is large brown and pink vug 6.1 to 7.2 cm below the top of the core. There is a small brown vug at the top of the core. There are no significant cracks, big voids, or mottling in the core.
	22	There is a large dark-brown vug 4.1 to 5.6 cm below the top of the core. There is a small dark-brown vug 2.8 to 3.5 cm below the top of the core. Minor subhorizontal pink altered regions containing small pores can be found throughout the core, but there are no large cracks or mottled areas.
h	20	There is a dark-brown subhorizontal vug 4.2 to 4.8 cm below the top of the core. There are small dark-brown vugs in a region from the top of the core to about 3 cm below the top mainly on one side. There are no significant horizontal voids or extensive mottled areas.
	6	There is a large dark-brown vug from the top of the core to 1 cm below the top. There is another large dark-brown vug 6.0 to 6.8 cm below the top of the core that has a light-pink altered region at the bottom edge of the brown vug. There are many small brown vugs in the core but no large-aperture voids and no significant mottled areas.

Pair	Core No.	Description
i	25	There is a subhorizontal vug 2.9 to 3.2 cm below the top of the core with a 1- to 2-mm aperture void, filled partly with pink altered material. There are no large brown inclusions, no extensive mottled areas.
	2	There is a very long subhorizontal vug 1.5 to 2.4 cm below the top of the core with white mineral filling and voids with 1- to 2-mm apertures. There is a subhorizontal vug at the bottom of the core with 1-mm aperture voids and pink mineral filling. There is a dark-brown inclusion 5 to 6 cm below the top of the core.
j	26	The core has a horizontal vug 0.1 to 0.4 cm from the top. The aperture is 1 mm, and the vug has some white mineral filling. There are other horizontal vugs 3.3 cm, 4.2 cm, and 4.8 to 5.0 cm from the top with hairline apertures. There is a horizontal vug with white mineral filling about 3 cm from the top. There are micropores in the filling. A dark-brown inclusion with a subhorizontal crack having a 0.5-mm aperture is about 5.5 to 6.2 cm from the top of the core.
	40	There are minor horizontal cracks at 3.5 cm and 4.1 cm from the top of the core with apertures 0.5 to 1 mm. There is a subvertical crack with a hairline aperture going from the top of the core to about 3.5 cm below the top and running into the horizontal crack described above. There is a large dark-brown inclusion about 3.9 to 4.7 cm from the top of the core.
k	30	There is a major vug about 3 cm below the top of the core. The subhorizontal void in the vug has an aperture of 1 to 1.5 mm. The vug is partly filled with a brownish-gray altered material. There is a subhorizontal vug at the top of the core with a void having a 1-mm aperture. The vug is partly filled with light-pink altered material containing small pores. There is a minor dark-brown vug 6.5 to 7.2 cm below the top of the core. It has subhorizontal voids having hairline to 0.5-mm apertures. The top of the core is mottled pink and brown.
	3	There is a major subhorizontal vug 3 to 4 cm from the top of the core, with voids that have approximately 1-mm apertures. The vug is partly filled with pink altered material and also with a dark-brown mineral. There is a minor subhorizontal vug 0.5 to 0.9 cm below the top of the core with voids with 1-mm aperture. There is a minor subhorizontal vug at the bottom of the core with a white mineral filling and a void with an aperture of about 0.5 mm.

Pair	Core No.	Description
l	31	There is a partly open hairline vertical crack 4.1 cm from the top of the core to the bottom of the core. There is a dark-brown vug 3.1 to 3.9 cm from the top of the core. There are subhorizontal dark-brown vugs 5.0 to 5.4 cm from the top of the core and 6.7 to 7.1 cm from the top of the core. There is a pink and brown vug at the top of the core and a pink and brown vug 0.6 to 2.1 cm from the top of the core.
	39	There is a partly open hairline to 1-mm aperture subvertical crack from the top of the core to 4.7 cm from the top of the core. There is a large pink void 0.3 to 1.5 cm from the top of the core. There are minor subhorizontal pink and light brownish-gray vugs near the center of the core.
m	33	There is a healed subvertical crack 5 cm from the top of the core to the bottom of the core. There is a small pink vug 1.2 to 1.9 cm from the top of the core, and a small pink vug 4.1 to 4.6 cm from the top of the core. There are no significant voids or dark-brown vugs and no mottled areas.
	32	There is a pink and light-brown inclusion 0.6 to 2 cm from the top of the core. The top 3 cm of the core show slight mottling. There is a healed hairline subvertical crack from the bottom of the core to 5.0 cm from the top of the core. There are no significant voids or dark-brown vugs.
n	41	There are parallel subhorizontal vugs 0.3 cm and 0.5 to 0.7 cm below the top of the core. The apertures of the voids are about 1 to 1.5 mm. There is a subvertical hairline crack from the top of the core to about 2.3 cm below the top of the core. There are brown vugs about 0.5 to 1.3 cm below the top of the core, 2.7 to 3.6 cm below the top of the core (including voids with 0.5-mm apertures), and 6.4 to 7.1 cm below the top of the core.
	35	There is a subhorizontal vug about 5 cm below the top of the core with a void having a 1- to 2-mm aperture. There is a hairline subvertical crack from 2.7 cm below the top of the core to the bottom of the core. There is a subhorizontal vug with a 0.5-mm aperture void about 0.5 to 0.7 cm below the top of the core. The top of the core is mottled pink and light grayish-brown.
o	44	There is a subhorizontal pink and brown vug 2.4 to 3.2 cm below the top of the core that contains hairline subhorizontal voids. There is a brown vug at the top of the core. There are small pink and brown vugs throughout the core.
	15	There are small brown and pink subhorizontal vugs throughout the core; there are minor subhorizontal voids with 0.5-mm apertures at 5.0 to 5.5 cm below the top of the core and at 6.4 to 7.0 cm from the top.

Pair	Core No.	Description
		Control Samples
p	5	There is a light-brown mottled region on the top 3 cm of one side of the core. There are minor pink subhorizontal vugs near the middle of the core. There are no voids and no dark-brown vugs.
	29	There is a minor light-brown mottled region in the top 3.5 cm of one side of the core. There is a small pink subhorizontal vug 6.5 to 6.7 cm from the top of the core that has a hairline subhorizontal crack. There are no dark-brown inclusions or other voids.
q	13	There is a major subhorizontal vug 3.5 to 4.2 cm below the top of the core with a void that has an aperture of 2 mm. The vug is partly filled with a white to pink altered material. There is a dark-brown vug 6.3 to 7.1 cm below the top of the core that contains hairline subhorizontal voids.
	42	There is a major subhorizontal vug 4.5 to 5.0 cm below the top of the core that has voids having 1- to 1.5-mm aperture. The voids are partly filled with light altered material. There is a minor subhorizontal vug at the top of the core with 1-mm aperture voids. Minor subhorizontal voids with hairline to 0.5-mm apertures are present throughout the core.
r	17	Core has a horizontal vug about 4.5 to 5.0 cm below the top of the core. Vug is filled with pink altered material and has voids with apertures of about 1 mm. Core has a dark-brown inclusion about 6.0 to 6.7 cm down from top and another dark-brown inclusion at the bottom of the core.
	34	Core has a very small horizontal vug about 5.0 to 5.5 cm from the top of the core with voids having apertures less than 0.5 mm. The vug is filled with light-pink to gray altered material. The core has a minor horizontal crack about 3.7 cm down from the top; the crack has a hairline aperture. There are dark-brown inclusions about 0.2 to 0.8 cm below the top, about 4.0 to 4.5 cm below the top, and just below the horizontal vug at 5.0 to 5.7 cm from the top.
s	19	There is a subhorizontal vug 3.2 to 4.2 cm below the top of the core that is partly filled with pink and white altered material and that has voids with 0.5- to 1.0-mm aperture. No large brown inclusions and no extensive mottled areas are present in the core. There is a hairline vertical crack from the top of the core to the bottom of the core.
	23	There is a subhorizontal vug 3.2 to 4.2 cm below the top of the core that is partly filled with pink and white altered material and that has voids with 0.5- to 1.0-mm aperture. No large brown inclusions and no extensive mottled areas are present in the core. There is a hairline vertical crack from the top of the core to the bottom of the core.
n/a	21	From the top of the core to about 2.3 cm from the top, there is a zone of open subhorizontal cracks with apertures of about 0.5 to 2 mm. This zone is mottled pink and brown. There is a brown and pink subhorizontal vug 4.3 to 5.0 cm below the top of the core and a pink vug 6.0 to 6.5 cm below the top of the core.

Appendix B:
Stress-Strain Plots for
Homogeneous and Heterogeneous Pairs

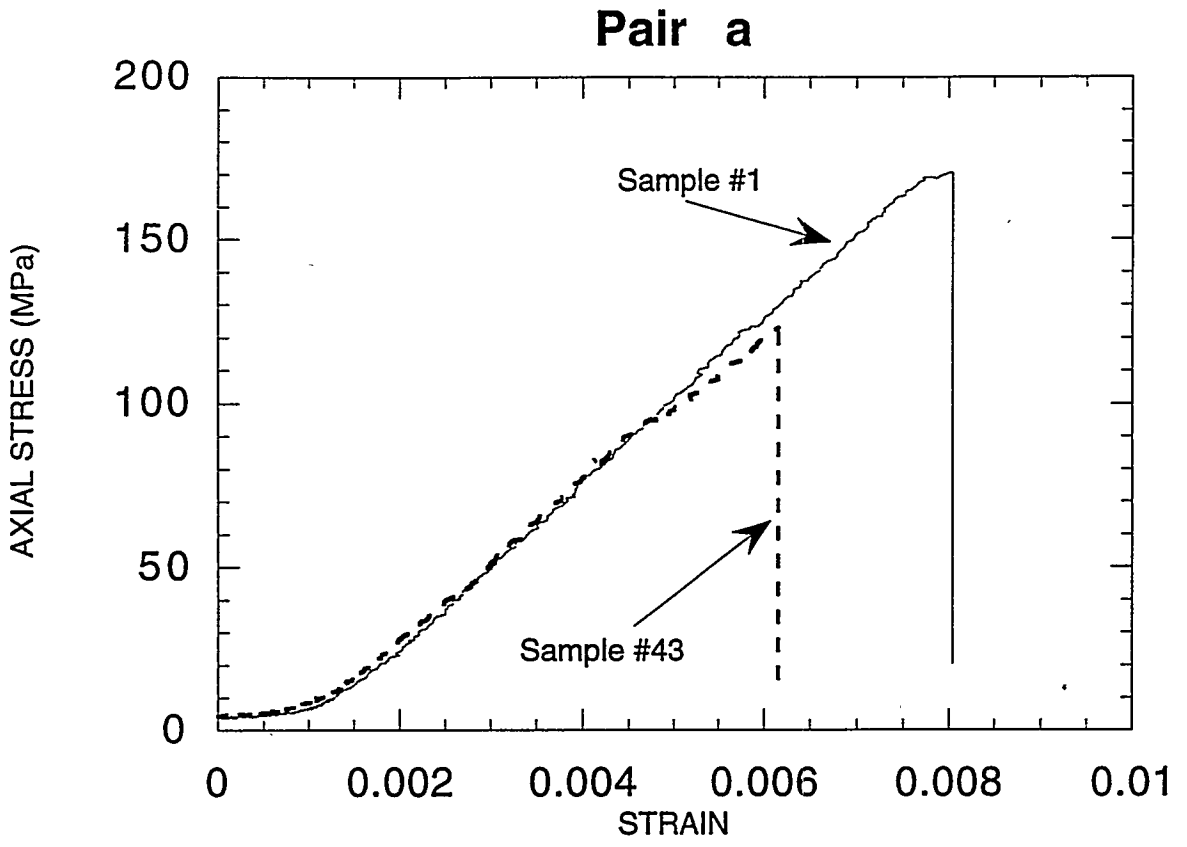
Pair a
AXIAL STRESS (MPa)
200
150
100
50
0
Sample #1
Sample #43
0
0.002
0.004
0.006
0.008
0.01
STRAIN

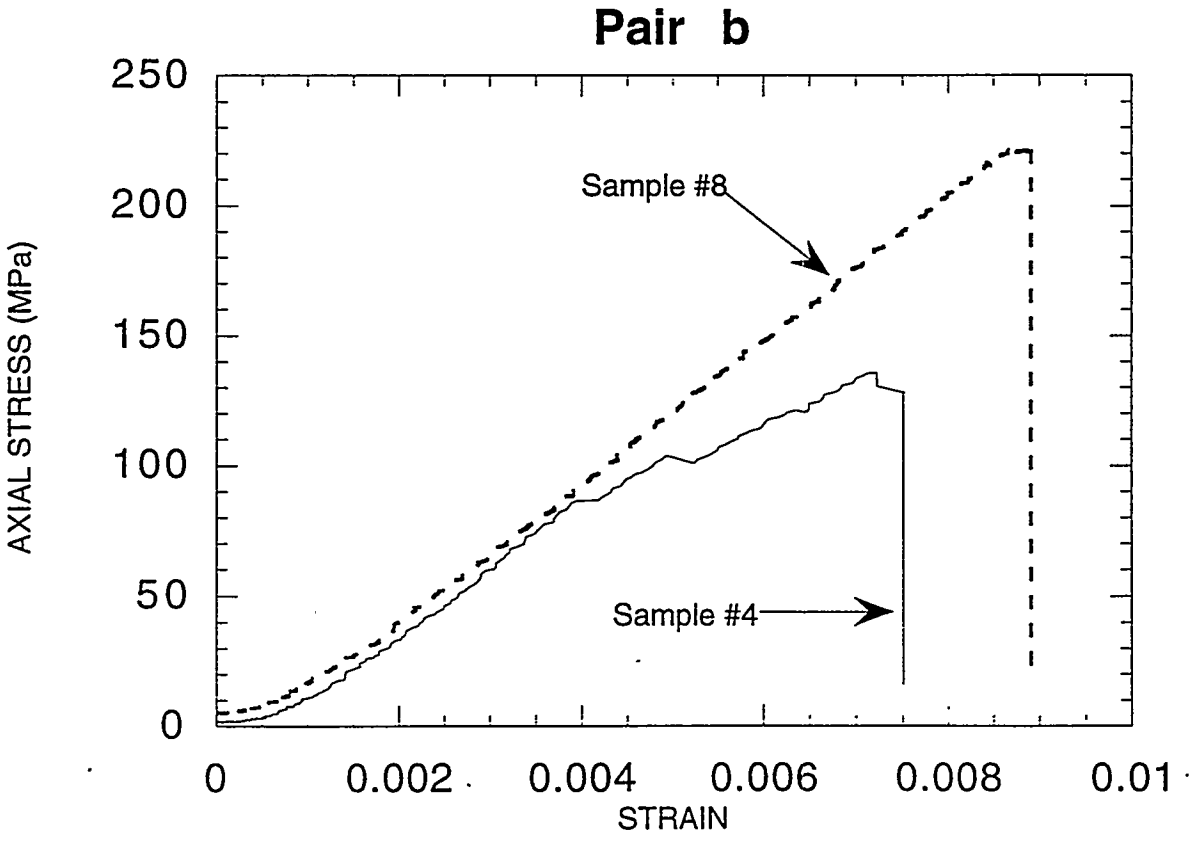
Pair b
AXIAL STRESS (MPa)
250
200
150
100
50
0
Sample #8
Sample #4
0
0.002
0.004
0.006
0.008
0.01
STRAIN

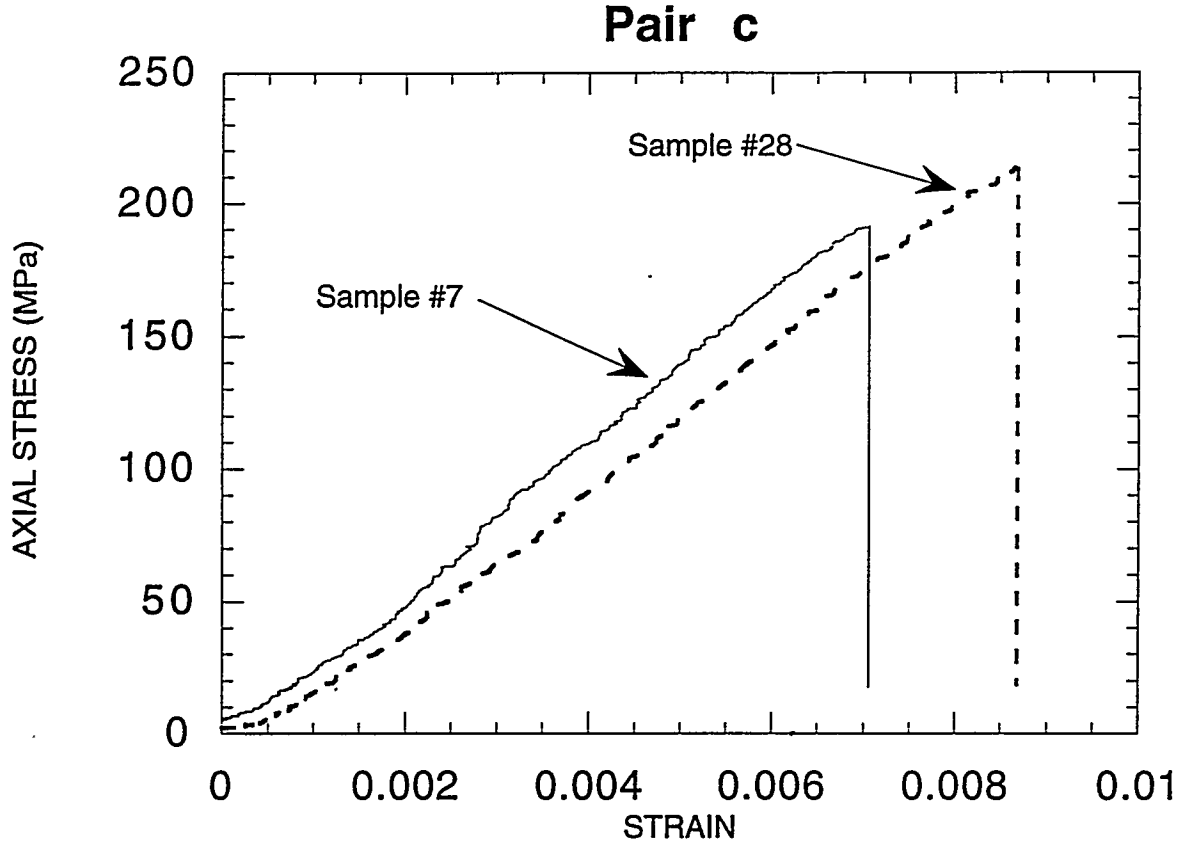
Pair c
250
200
150
100
50
0
AXIAL STRESS (MPa)
Sample #28
Sample #7
0
0.002
0.004
0.006
0.008
0.01
STRAIN

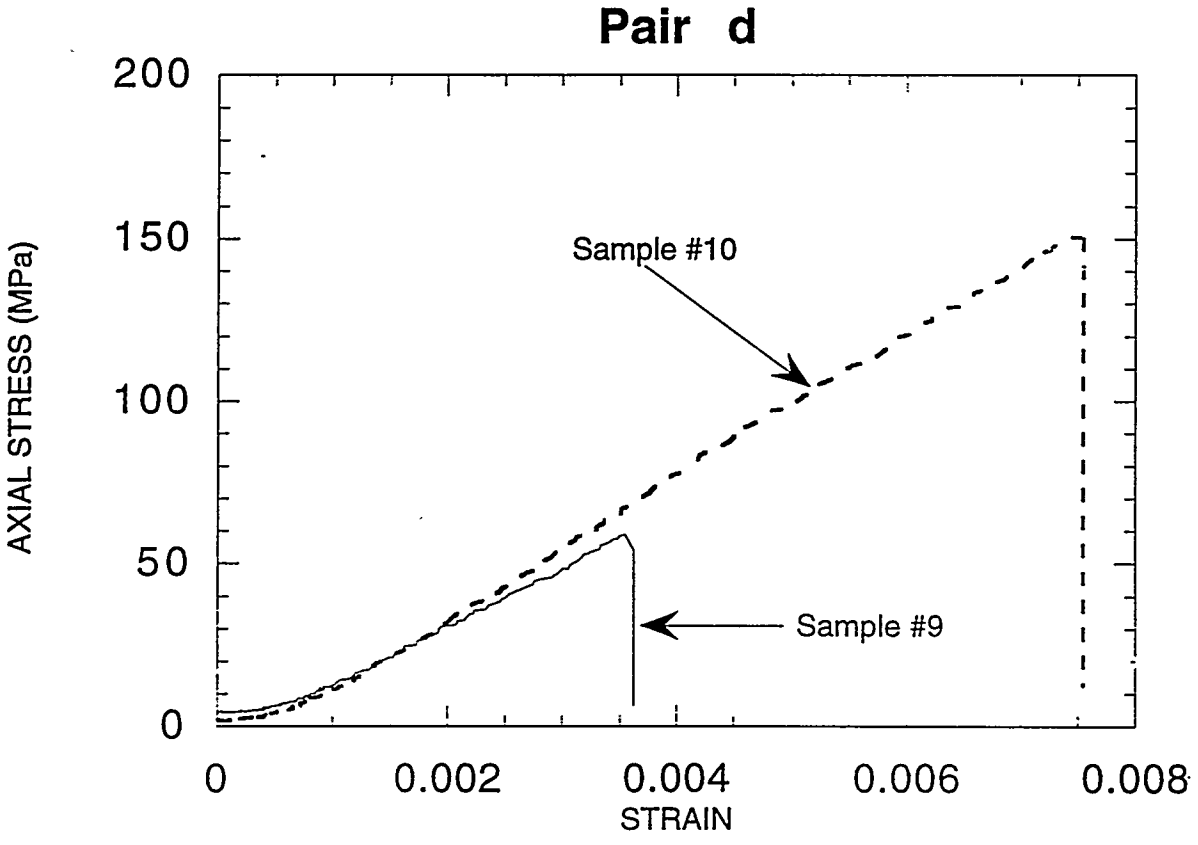
Pair d
200
150
100
50
0
AXIAL STRESS (MPa)
Sample #10
Sample #9
0
0.002
0.004
0.006
0.008
STRAIN

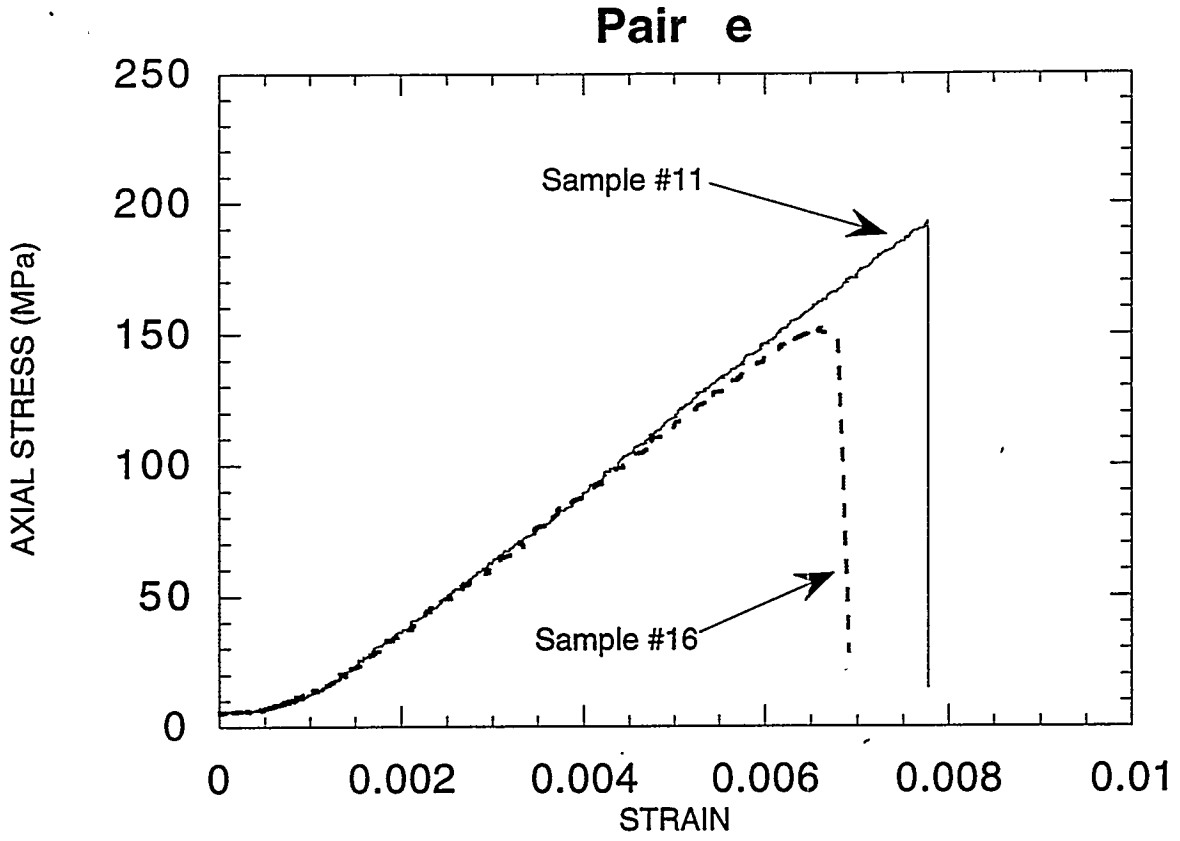
Pair e
AXIAL STRESS (MPa)
250
200
150
100
50
0
Sample #11
Sample #16
0
0.002
0.004
0.006
0.008
0.01
STRAIN

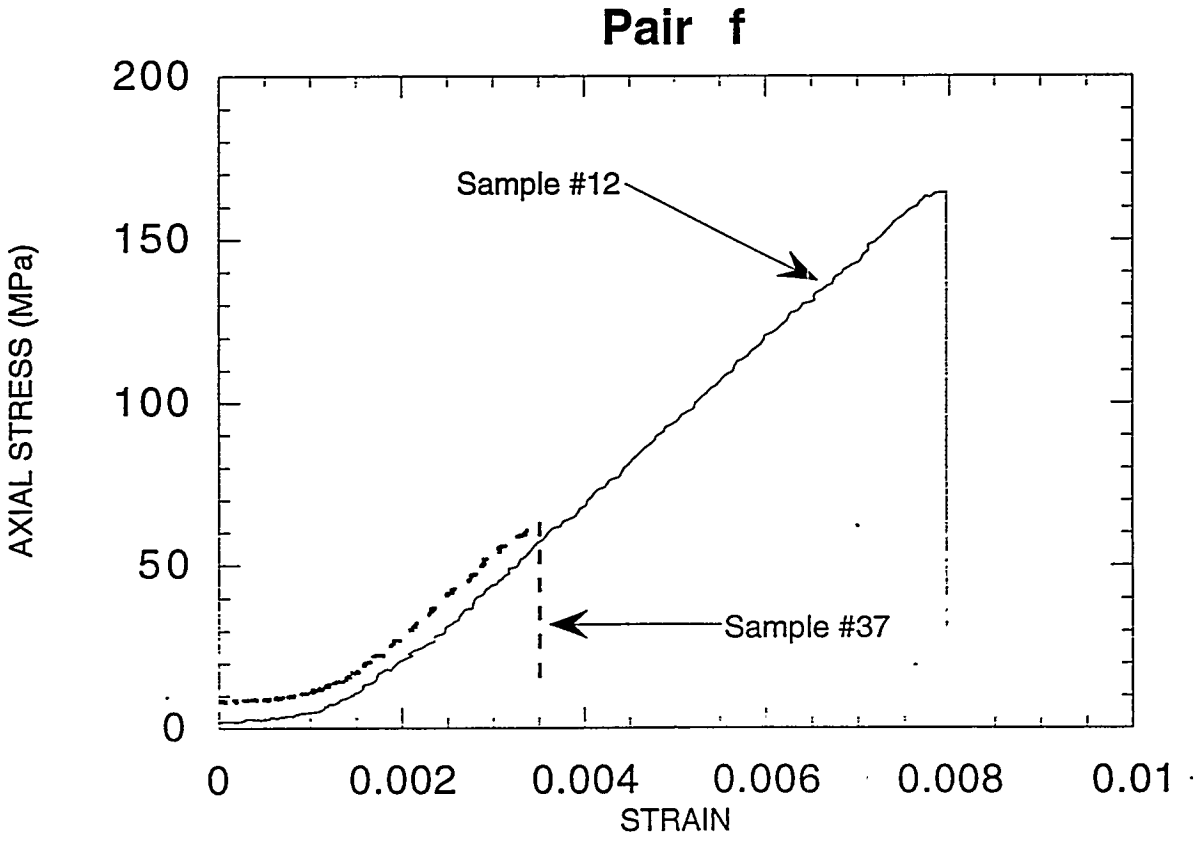
Pair f
AXIAL STRESS (MPa)
200
150
100
50
0
Sample #12
Sample #37
0
0.002
0.004
0.006
0.008
0.01
STRAIN

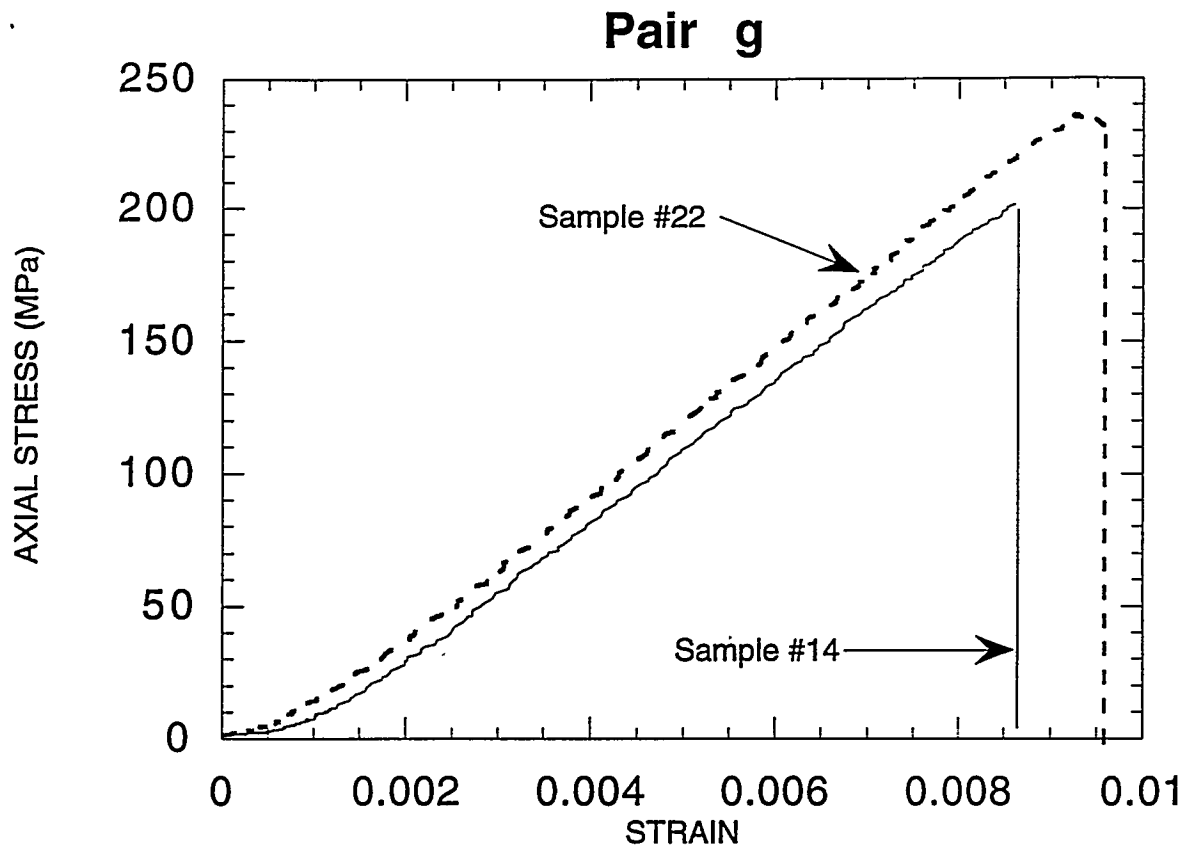
Pair g
AXIAL STRESS (MPa)
250
200
150
100
50
0
Sample #22
Sample #14
0
0.002
0.004
0.006
0.008
0.01
STRAIN

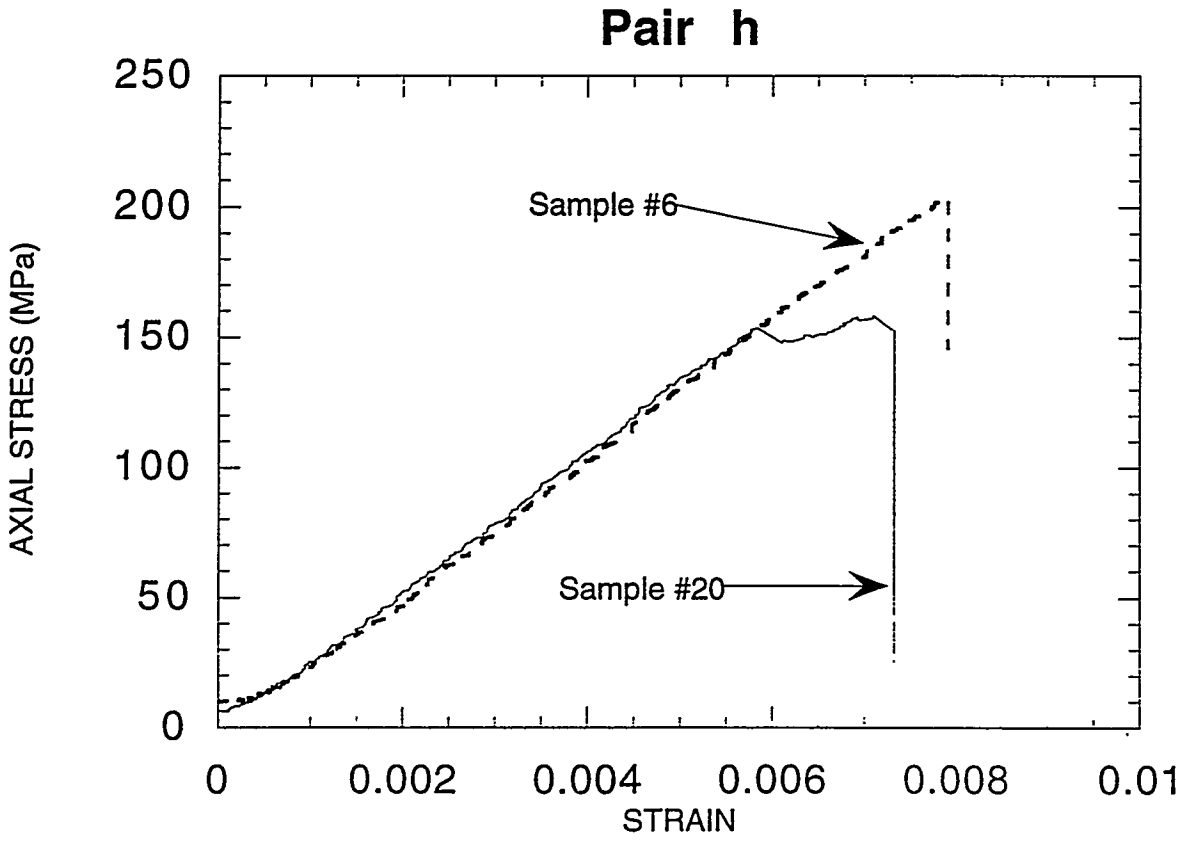
Pair h
AXIAL STRESS (MPa)
250
200
150
100
50
0
Sample #6
Sample #20
0
0.002
0.004
0.006
0.008
0.01
STRAIN

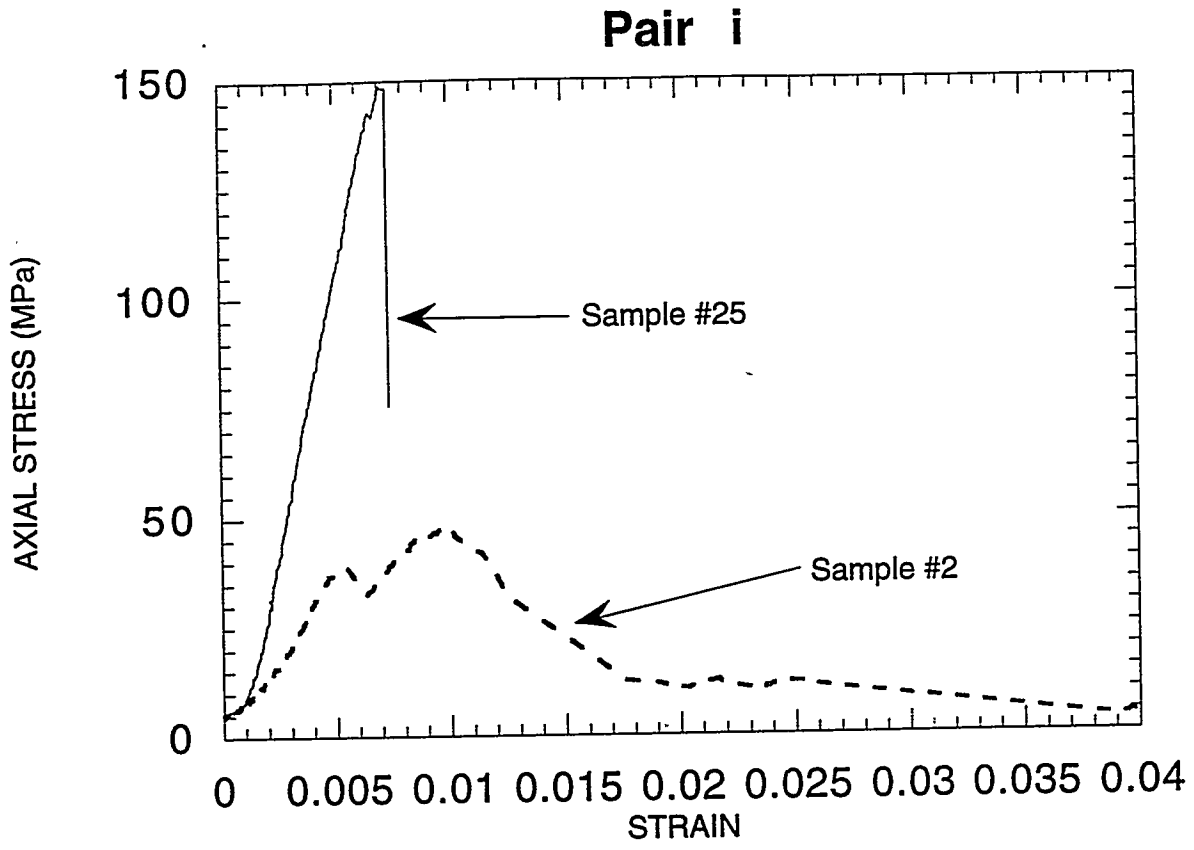
Pair i
150
100
50
0
AXIAL STRESS (MPa)
Sample #25
Sample #2
0 0.005 0.01 0.015 0.02 0.025 0.03 0.035 0.04
STRAIN

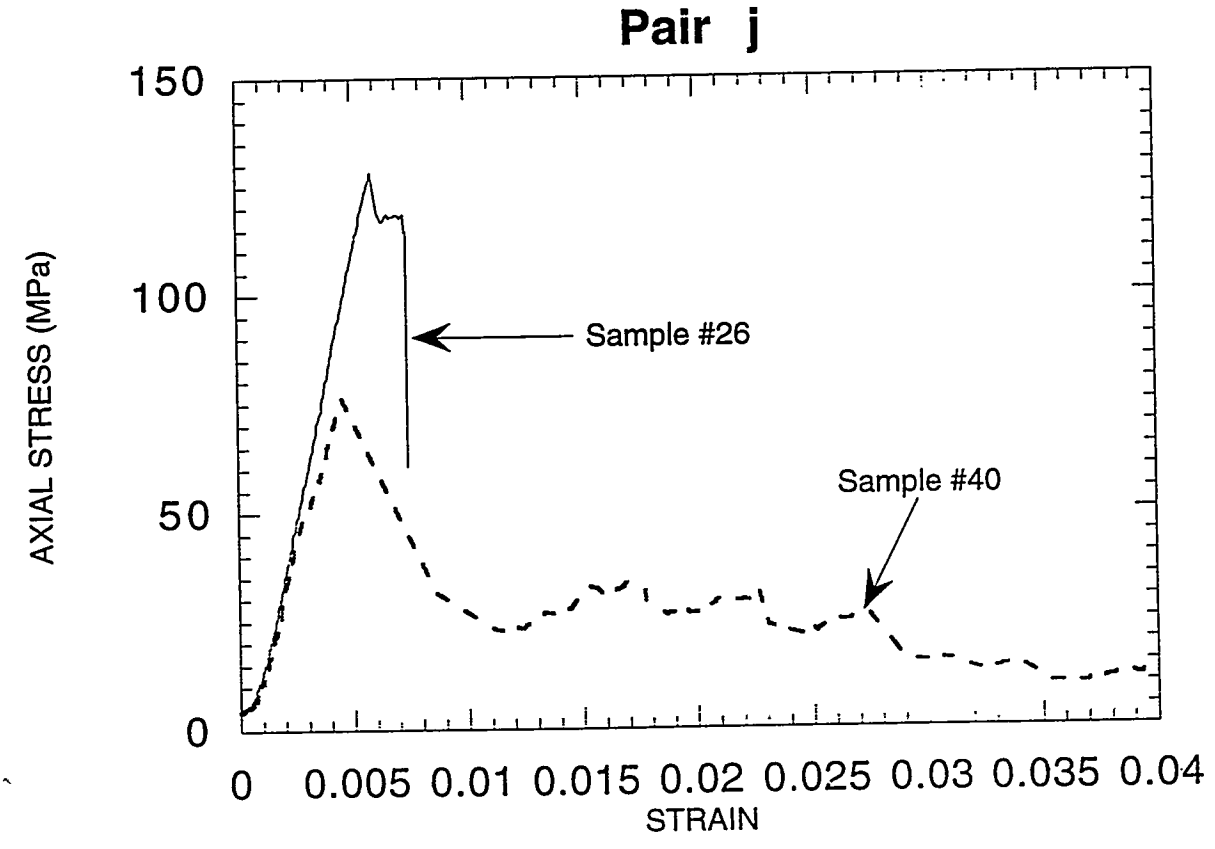
Pair j
150
100
50
0
AXIAL STRESS (MPa)
Sample #26
Sample #40
0 0.005 0.01 0.015 0.02 0.025 0.03 0.035 0.04
STRAIN

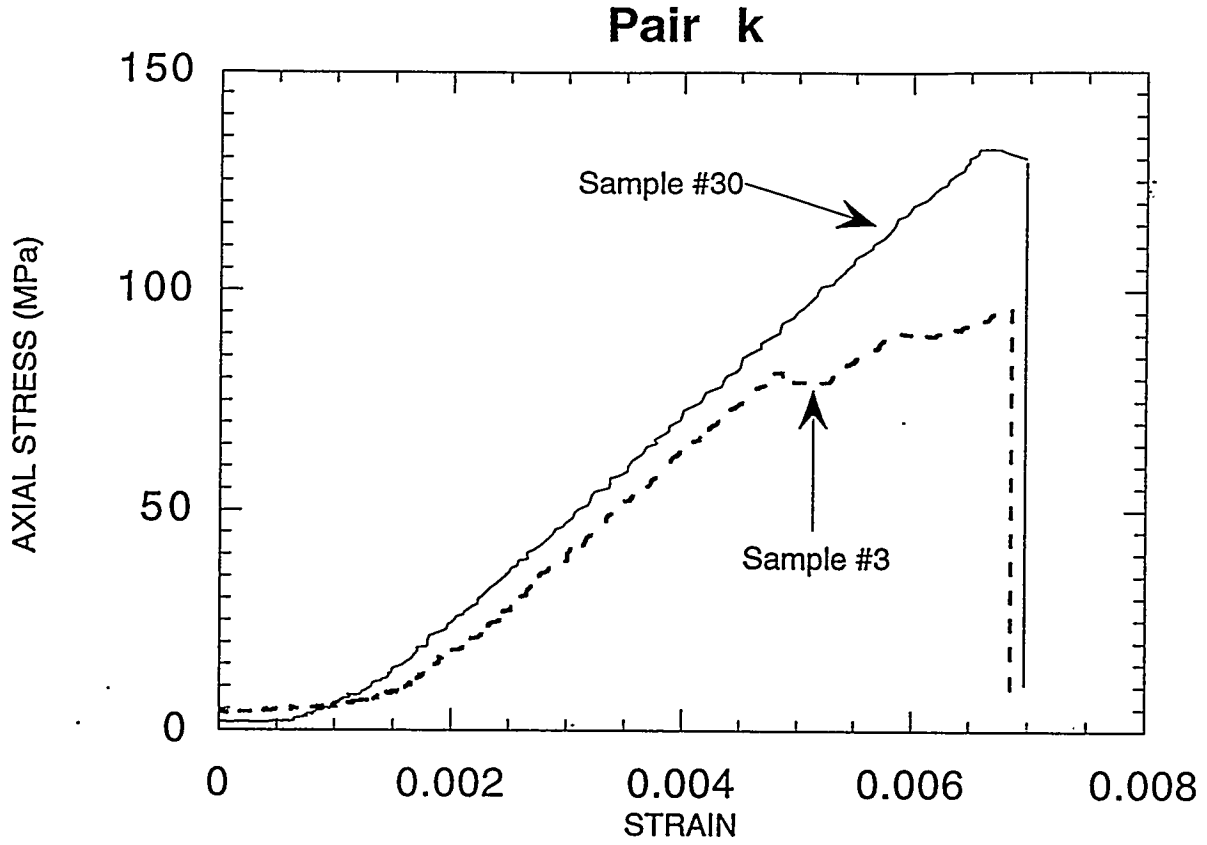
Pair k
150
100
50
0
AXIAL STRESS (MPa)
Sample #30
Sample #3
0
0.002
0.004
0.006
0.008
STRAIN

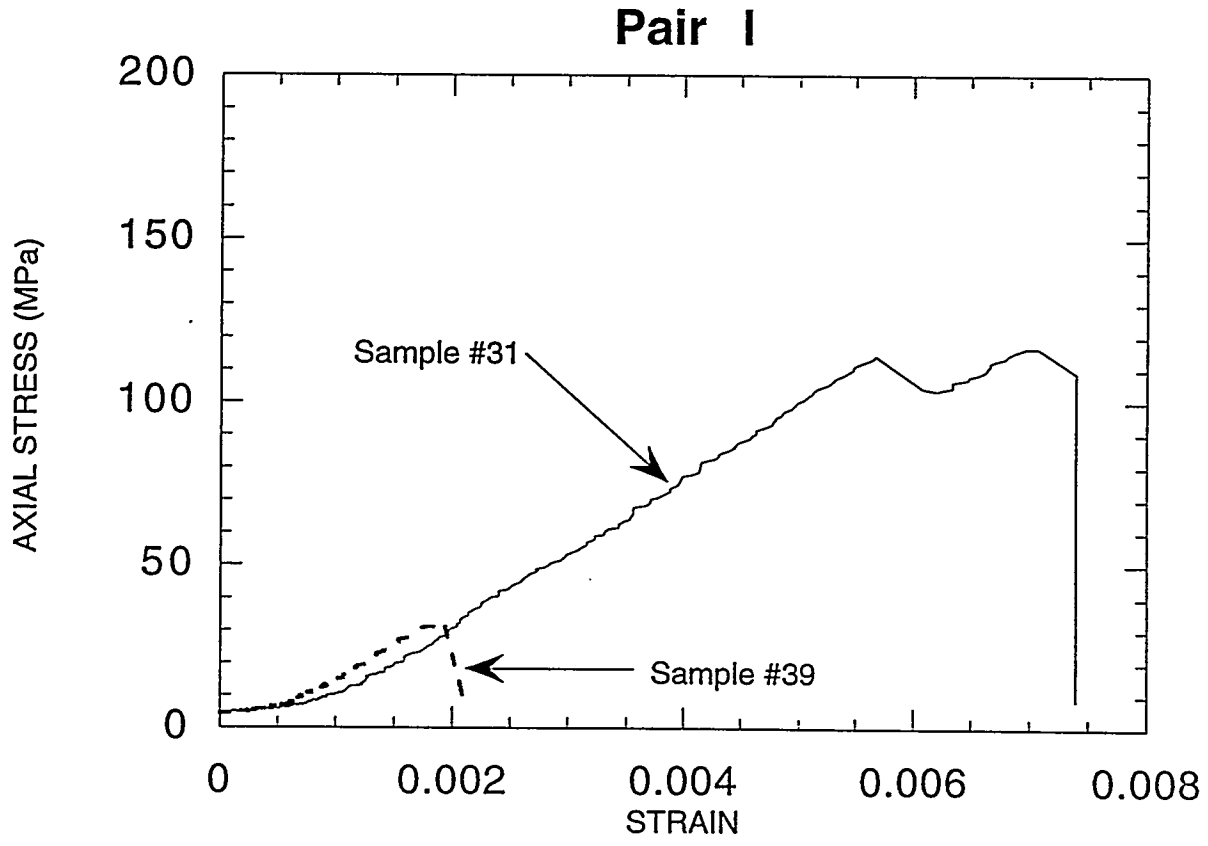
Pair l
200
150
100
50
0
AXIAL STRESS (MPa)
Sample #31
Sample #39
0
0.002
0.004
0.006
0.008
STRAIN

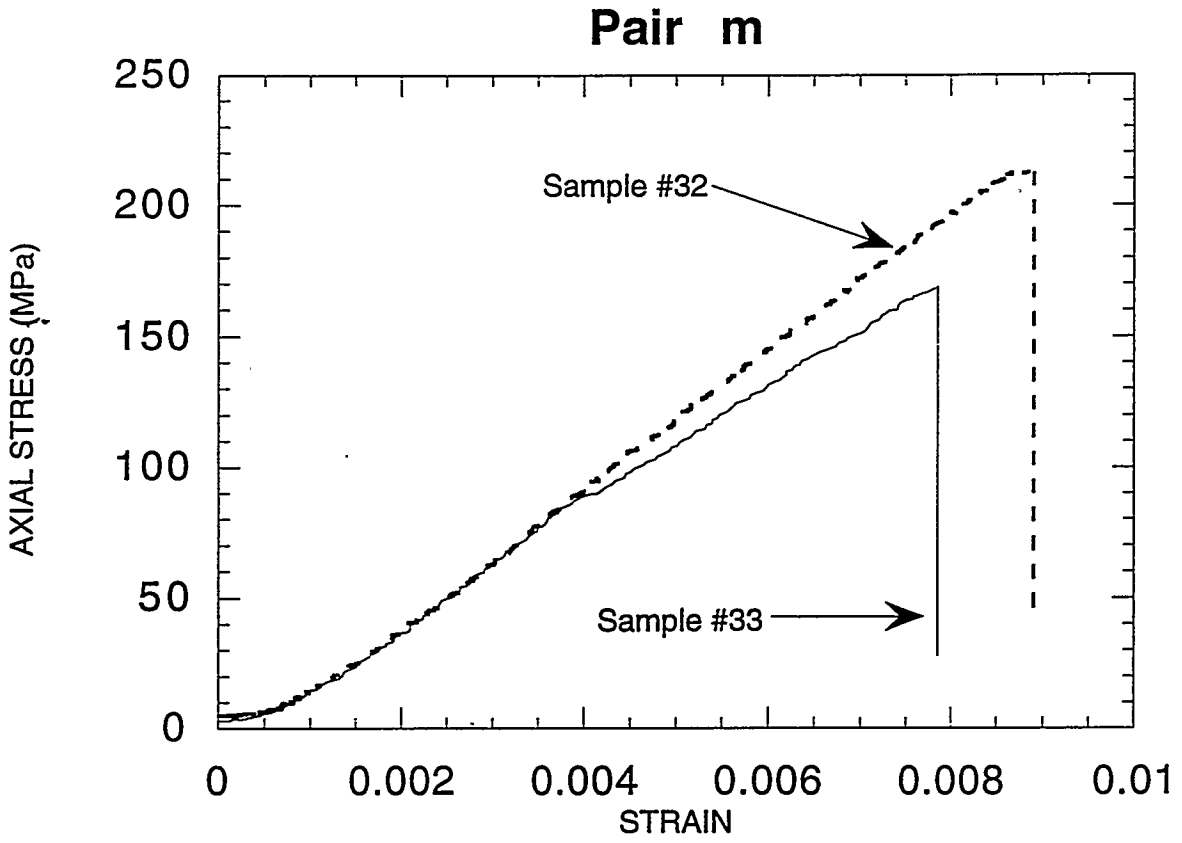
Pair m
AXIAL STRESS (MPa)
250
200
150
100
50
0
Sample #32
Sample #33
0
0.002
0.004
0.006
0.008
0.01
STRAIN

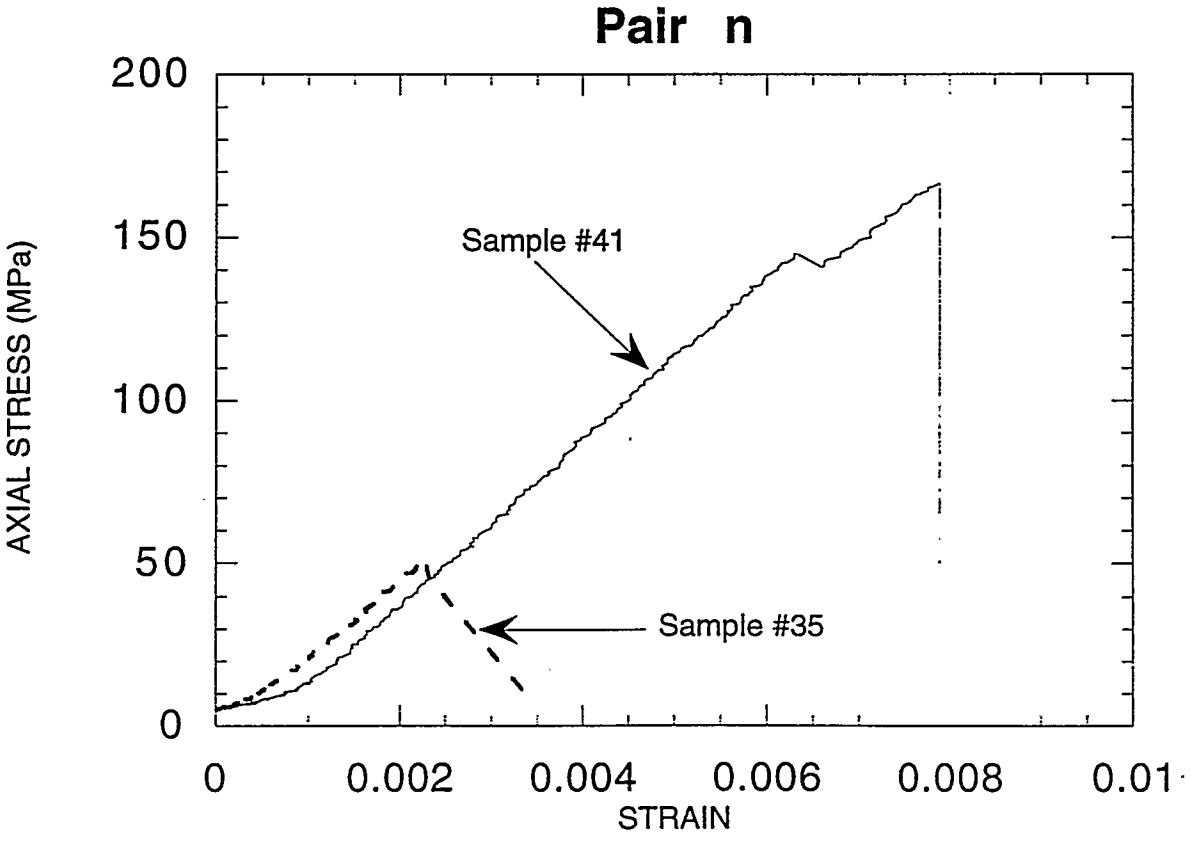
Pair n
AXIAL STRESS (MPa)
200
150
100
50
0
Sample #41
Sample #35
0
0.002
0.004
0.006
0.008
0.01
STRAIN

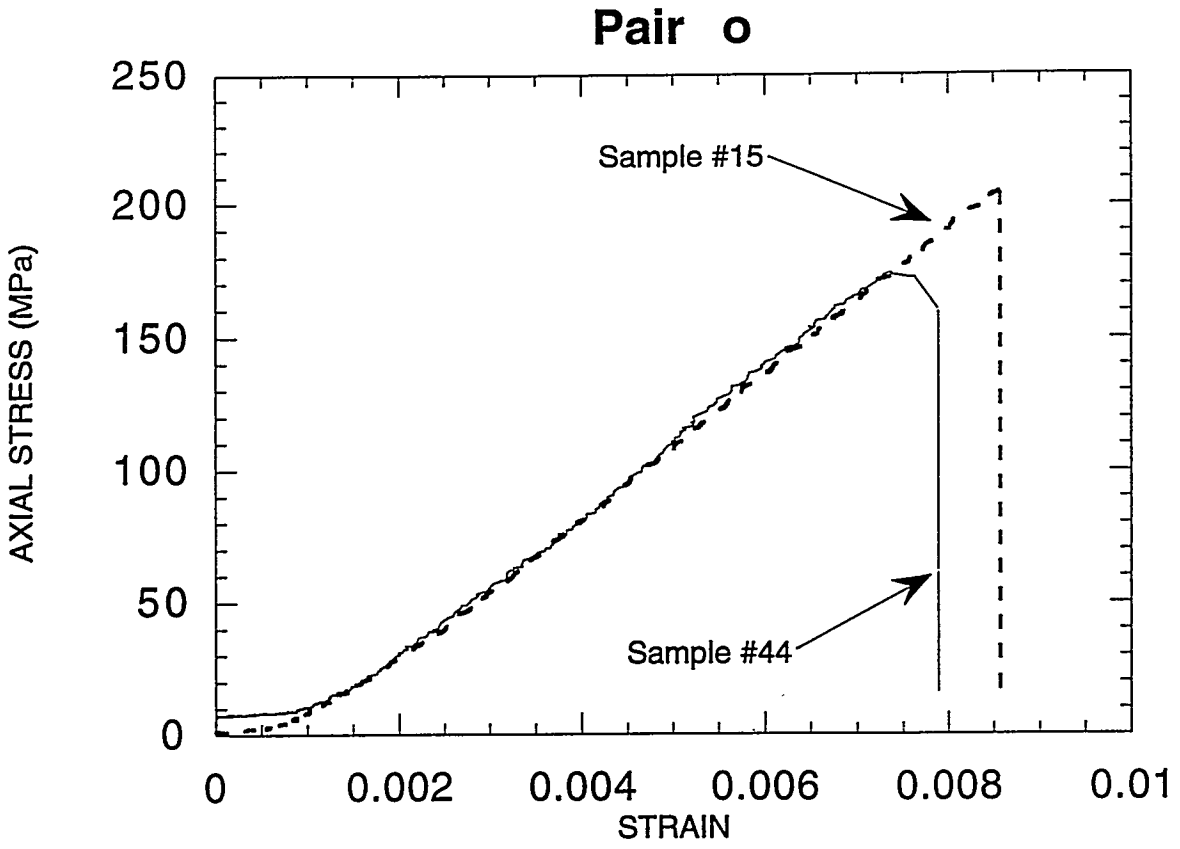
Pair o
250
200
150
100
50
0
AXIAL STRESS (MPa)
Sample #15
Sample #44
0
0.002
0.004
0.006
0.008
0.01
STRAIN